IEEE Photonics Journal
An IEEE Photonics Society Publication

Tunable and Multiple Plasmon-Induced Transparency in a Metasurface Comprised of Silver S-Shaped Resonator and Rectangular Strip

Volume 12, Number 3, June 2020

R. M. H. Bilal
M. A. Baqir
P. K. Choudhury, *Senior Member, IEEE*
M. M. Ali
A. A. Rahim

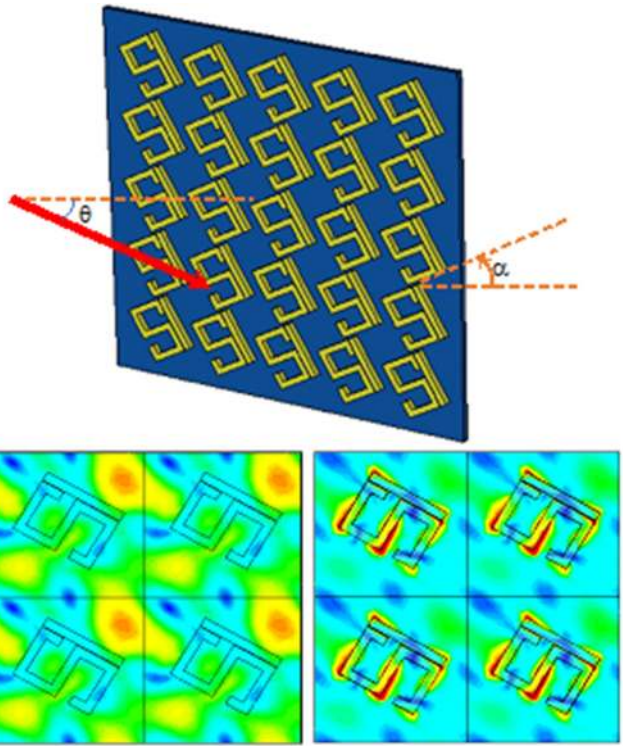

DOI: 10.1109/JPHOT.2020.2988698

Tunable and Multiple Plasmon-Induced Transparency in a Metasurface Comprised of Silver S-Shaped Resonator and Rectangular Strip

R. M. H. Bilal,[1] M. A. Baqir,[2] P. K. Choudhury,[3] *Senior Member, IEEE*, M. M. Ali,[4] and A. A. Rahim[1]

[1]Faculty of Electrical Engineering, Ghulam Ishaq Khan Institute of Engineering Sciences and Technology, Topi, Khyber Pakhtunkhwa 234640, Pakistan
[2]Department of Electrical and Computer Engineering, COMSATS University Islamabad Sahiwal Campus, 57000, Pakistan
[3]Institute of Microengineering and Nanoelectronics, Universiti Kebangsaan Malaysia, UKM Bangi 43600 Selangor, Malaysia
[4]Department of Electronic and Computer Engineering, University of Limerick, V94 T9PX Limerick, Ireland

DOI:10.1109/JPHOT.2020.2988698

Manuscript received April 7, 2020; accepted April 15, 2020. Date of publication April 21, 2020; date of current version May 26, 2020. This work was supported by the Ministry of Higher Education (MOHE), Malaysia under Grant FRGS/1/2019/STG02/UKM/01/1. Corresponding author: P.K. Choudhury (e-mail: pankaj@ukm.edu.my).

Abstract: The plasmon-induced transparency (PIT) in planar metasurface comprising of resonators having one S-shaped structure and a rectangular strip (both made of silver) was investigated. It was found that the S-shaped component of metasurface induces a single bright mode, whereas the rectangular strip manifests two bright modes with strong coupling of incidence electromagnetic waves. When both the metasurface components were placed in the proximity, the PIT-like phenomenon was observed. The effects of rotational angle of the metasurface as well as the angle of incidence on the transmission spectra (of the metasurface) were also investigated. Both the transverse electric (TE) and transverse magnetic (TM) waves were used to explore the PIT effect. It was noticed that the PIT window could be easily tuned by altering the horizontal distance between the resonator components (i.e., the S-shaped structure and rectangular strip). It is expected that the proposed metasurface structure would be prudent in switching, ultrafast sensing and optical applications.

Index Terms: Plasmon-induced transparency, metasurface, resonating structures.

1. Introduction

2D metamaterials of sub-wavelength size thickness reveal fantastic and unique light controlling capabilities [1]–[4]. Metasurface-based devices are ultrathin and miniaturized, which distinguish these from the conventional bulky optical devices, thereby making these attractive for future optical applications [5], [6]. Due to the unusual features of metasurfaces, these find promising potentials in constructing waveplates [7], [8], planar lenses [9], [10], beam splitters [11], planar filters [12], [13], modulators [14]–[16], meta-holograms [17]–[19], meta-switches [20], optical vortex and Bessel beam generation [21]–[24], etc. With the rapid advancements in nanotechnology, and in view of the

future challenges of optical communication systems, researchers have been developing varieties of not only photonic, but also plasmonic structures during the last few years.

Electromagnetically induced transparency (EIT) is the electromagnetic phenomenon that takes place in three-level atomic systems. This results owing to the interference of the atomic resonance [25], [26]. Plasmon-induced transparency (PIT) is the analogues of EIT, usually observed in metamaterial structures [27]–[29], and remains an attractive topic for research. PIT got widespread applications in optical storage devices [30], nano-sensing [31], filtering [32], optical switching [33], etc. PIT with narrow window remains useful for sensing and switching applications [34], [35]. Refs. [36], [37] illustrate potentials of PIT with high Q-factor in sensing. Switching applications of PIT have been reported in [38], [39].

Zhang *et al.* [27] firstly proposed the phenomenon of PIT in the terahertz (THz) regime in metamaterial comprised of two optical nano-antennas. The trapping of surface plasmon polariton (SPP) in metamaterial structures can break the diffraction limit and manipulate the electromagnetic waves at the sub-wavelength scale. This opens up a new horizon to realize many optical devices, such as detectors [40], polarizers [41], absorbers [42], [43], amplifiers [44], biosensors [45], [46], antennas [47] and filters [48], etc.

The phenomenon of PIT generally results in because of strong coupling between the bright-dark or bright-bright modes. Plenty of PIT-based designs have been implemented to develop metamaterials [49], nanowire gratings [50] and coupled waveguides [51]. Within the context, Chen *et al.* [52] observed the PIT-like switching response in plasmonic resonators composed of a metallic split-ring resonator (SRR) and rectangular strip. Liu *et al.* [31] demonstrated highly sensitive metamaterial-based sensor, which works on the PIT-like phenomenon. Yi *et al.* [53] proposed compact XOR and XNOR logic gates exploiting the PIT-based metamaterials.

Tunable and multiple PIT windows (TMPWs) are expedient as these find applications in nano-sensing and optical switching. These are usually created by the complex and multifaceted arrangements for fabrication [54]–[56], which limit their practicability. As such, it has been a challenging task to create TMPWs exploiting simple and compact structures.

In this paper, we investigate the characteristics of TMPWs in specially designed planar metasurface having the unit cell consisting of an S-shaped resonator and a rectangular strip, both made of silver. We study the electromagnetic response of the proposed PIT-like metasurface under different rotational angles of the resonators at the top. We observe multiple PIT windows with low and high amplitudes; the latter one being useful for THz sensing and future communication applications, such as modulation and switching. The effect of different oblique incidence angles on the transmission spectra is also determined. We consider both the transverse electric (TE) and transverse magnetic (TM) modes, and analyze the tuning feature (of the PIT window) by altering the horizontal distance between the resonator components. Further, the electric field and current distribution patterns are also plotted corresponding to different resonance conditions in the transmission spectra. Mestasurafces exhibiting single- and/or double-PIT windows have been communicated before in the literature. Ref. [57] demonstrates multiple PIT by using an arrangement of ring resonators. However, the design presented in this paper is simple, wherein multiple PIT windows could be obtained by the use of combinational arrangements of metallic strip and S-shaped resonators.

2. Design and Modeling

Fig. 1 illustrates the schematic of the two-layer planar metasurface-based structure, wherein the unit cell of the top metasurface has a suitable arrangement of an S-shaped resonator and a rectangular strip, both made of silver. This metasurface is grown over silicon dioxide (SiO_2) dielectric substrate. The S-shaped resonator and rectangular strip are placed at a distance S from each other, as shown in Fig. 1(a). Figs. 1(b) and (c), respectively, depict the three-dimensional (3D) and side views of the structure.

We obtain the optimized design parameters of the proposed PIT-based metasurface configuration; these are as $P = 80\ \mu$m, $L = 45\ \mu$m, $W = 5\ \mu$m, $a = 30\ \mu$m, $b = 25\ \mu$m, $c = 12.5$

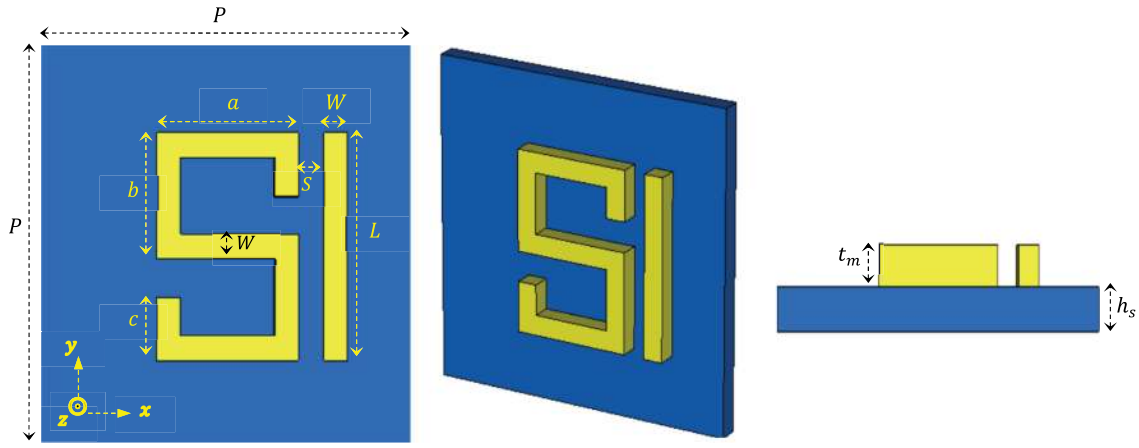

Fig. 1. Schematic diagram of the proposed PIT planar metasurface: (a) cross-sectional view, (b) 3D view, and (c) side view.

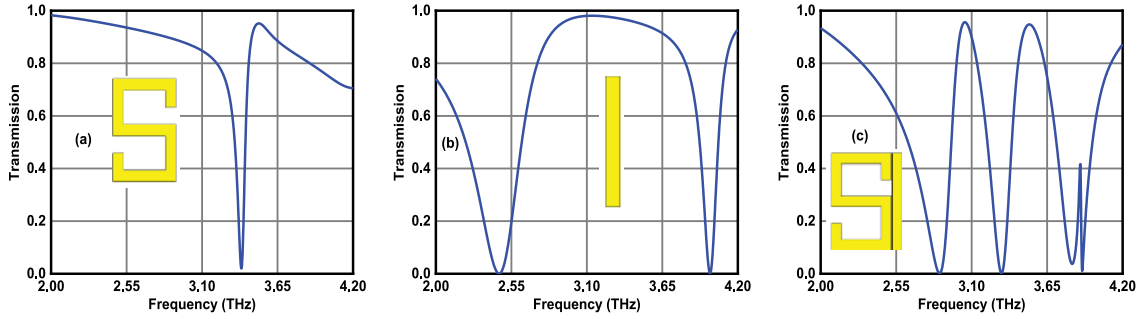

Fig. 2. Transmission spectra obtained upon using the individual components of the proposed metasurface; (a) S-shaped resonator, (b) rectangular strip, and (c) S-shaped resonator and rectangular strip together.

μm and $S = 0.5$ μm; Fig. 1(a) shows all these parametric symbols. The thickness of the top unit cell (t_m) and that of the dielectric substrate (h_s) are taken to be 5 μm each (Fig. 1(c)). Having these design considerations in mind, the proposed planar metasurface is simulated by using the commercially available 3D EM software CST Microwave Studio. We take the value of conductivity σ of silver as 6.3×10^7 S/m, as recorded from the software library. Apart from this, silver being dispersive in nature, its permittivity at 2 THz frequency is taken to be $(-1.77 + 3.87i) \times 10^5$ [58]. Also, the permittivity of SiO_2 is considered as 3.5. While performing simulations, we impose the unit cell boundary conditions along the *x*-*y* direction, and the open add space boundary conditions along the *z*-axis, above and below the proposed PIT device. The top plasmonic metasurface is illuminated with incidence EM wave from the $+z$-axis, and the transmission characteristics are noticed along the $-z$-axis.

3. Results and Discussion

Fig. 2 shows the transmission spectra of the proposed planar metasurface configuration. However, while obtaining these spectral characteristics, we initially take into account the resonator components (of the metasurface) individually, and excite those. Within the context, Fig. 2(a) corresponds to the transmission spectra of the silver S-shaped resonator only. In this figure, we observe the presence of a transmission dip at 3.40 THz. This corresponds to the bright mode, which is strongly coupled with the S-shape resonator. Fig. 2(b) illustrates the transmission spectra due to

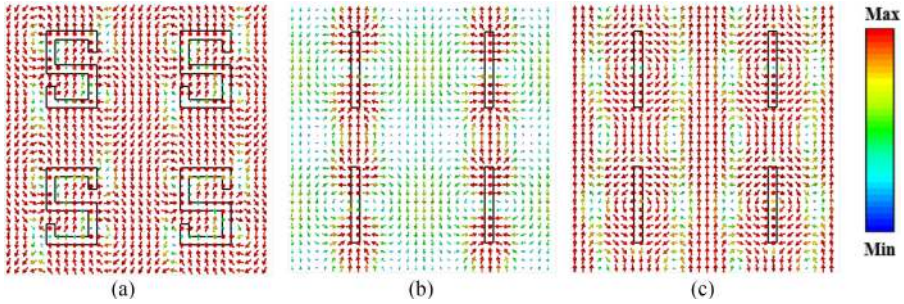

Fig. 3. Surface current density around the silver strip corresponding to (a) 3.40 THz (for S-shaped resonator), (b) 2.46 THz, and (b) 4.0 THz (for silver strip resonator).

the excitation of the rectangular silver strip only. We notice the presence of two transmission dips (with zero transmission) in this case, positioned at the frequency values of 2.46 THz and 4.0 THz. These two transmission dips are also named to be the bright modes. As such, the use of strip and S-shaped metallic resonators in forming metamaterials would be interesting owing to the feature of exhibiting multiple PIT windows – the phenomenon that results in due to the interactions of multiple bright-bright and bright-dark modes.

Fig. 3 illustrates the surface current distribution patterns corresponding to the cases when the S-shaped resonator and silver strip are used individually. Upon interaction with incidence electromagnetic waves, the dipolar response is observed in which the currents are flowing upward and downward alternately. As Figs. 2(a) and (b) exhibit the presence of transmission dips at the frequencies 3.40 THz, 2.46 THz and 4.0 THz, Figs. 3(a), 3(b) and (c), respectively, depict the surface current distribution patterns corresponding to these values of frequency, thereby determining bright modes. We find that, in the case of S-shaped resonator, the current density remains maximum on the surface of the resonator (Fig. 3(a)), which confirms the presence of bright modes. We further notice that, in the case of bright mode at 2.46 THz, the strong current density exists at the surface of the metallic strip, and it becomes weaker upon moving away from the resonator (Fig. 3(b)). Corresponding to the transmission dip positioned at 4.0 THz, the surface current remains more confined around the resonator (Fig. 3(c)).

When both the metasurface components are excited together in a certain arrangement, as shown in Fig. 2(c), strong coupling between the S-shaped resonator and rectangular strip occurs, which remains responsible for the generation of PIT effect in the metasurface. Fig. 2(c) depicts the transmission spectra obtained in this case. We find the presence of dips in the transmission spectra positioned at 2.86 THz, 3.33 THz, 3.83 THz, 3.90 THz; the respective transmission peaks appear at the frequency values of 3.05 THz, 3.50 THz, 3.88 THz. We clearly notice that the resonance condition is greatly altered upon amalgamating the components which the unit cell is comprised of. Both the resonators have strong coupling, and the PIT windows appear due to destructive interference of PIT bright modes. Considering the transmission dips as observed in Fig. 2(c), we present the surface current density patterns in Fig. 4. Here Figs. 4(a), 4(b), 4(c) and 4(d), respectively, exhibit current distributions corresponding to the values of frequency 2.86 THz, 3.33 THz, 3.83 THz and 3.90 THz. From these figures, the coupling between the two resonator elements in the metasurface becomes obvious.

We now attempt to investigate the impact of rotating the metasurface components when the S-shaped structure and rectangular strip are placed together in the proximity, i.e., the kind on configuration used in Fig. 2(c). We consider the angle of rotation to be α, and observe the results when α assumes values as 30°, 45°, 60° and 90°, and also, taking into account the excitations by the TE- and TM-polarized waves. Fig. 5 illustrates the schematic of the array of unit cell that forms the metasurface. In this figure, θ and α represent the angles of incidence and rotation (of metasurface), respectively.

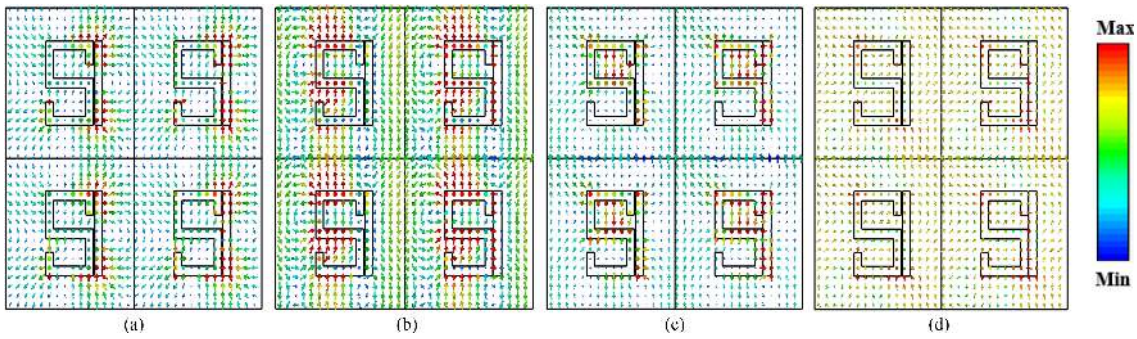

Fig. 4. Surface current density in the case when the S-shaped resonator and rectangular strip are used together, as shown in Fig. 2(c).

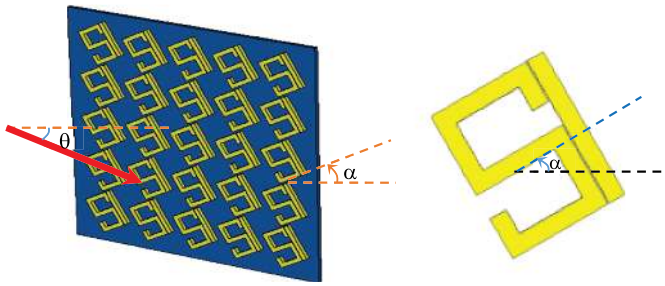

Fig. 5. Schematic of the proposed metasurface along with the angular representations.

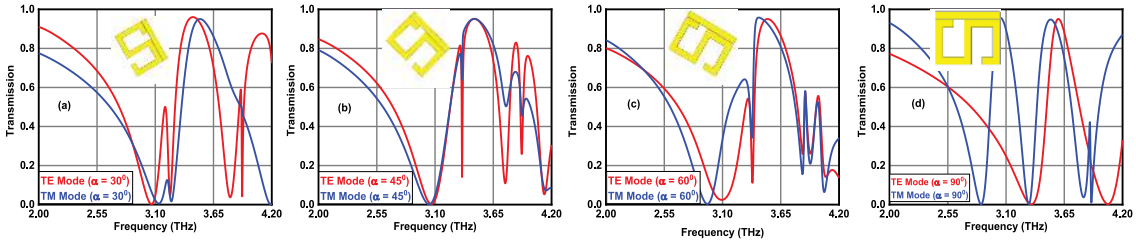

Fig. 6. Simulated transmission spectra of the proposed metasurface under various rotational angles of the top resonators: (a) $\alpha = 30°$, (b) $\alpha = 45°$, (c) $\alpha = 60°$, and (d) $\alpha = 90°$.

Fig. 6 shows the transmission spectra obtained in this case. Indeed, the spectral characteristics are significantly altered upon implementing such a rotation. In particular, under the TE-polarized incidence excitation, the use of $\alpha = 30°$ exhibits four PIT peaks positioned at the frequency values of 3.19 THz, 3.45 THz, 3.90 THz and 4.05 THz (Fig. 6(a)). However, a TM-polarized excitation yields one PIT peak at the frequency of 3.5 THz. As such, the number of PIT peaks is reduced while changing the excitation mode from the TE-polarized to the TM-polarized one. However, the same in not observed upon increasing the angle to 45°, as can be seen in Fig. 6(b). In this case, both the TE- and TM-polarized incidence excitations yield four PIT peaks corresponding to four different resonance frequencies, and for each type of polarization, the obtained PIT peaks are positioned at almost the same frequency. In this case, the transmission in the higher frequency regime (above 3.7 THz) remains significantly large (with relatively sharper transmission peaks) for the TE mode, as compared to the TM.

Upon increasing the angle of rotation of the unit cell (in the top metasurface) to 60°, we notice in Fig. 6(c) that both the TE- and TM-mode excitations yield four PIT peaks at the operating frequencies of nearly at 3.34 THz, 3.88 THz, 4.0 THz and 4.13 THz. But, corresponding to higher frequencies above 3.7 THz, the transmittance is significantly reduced. Making $\alpha = 90°$ results in the

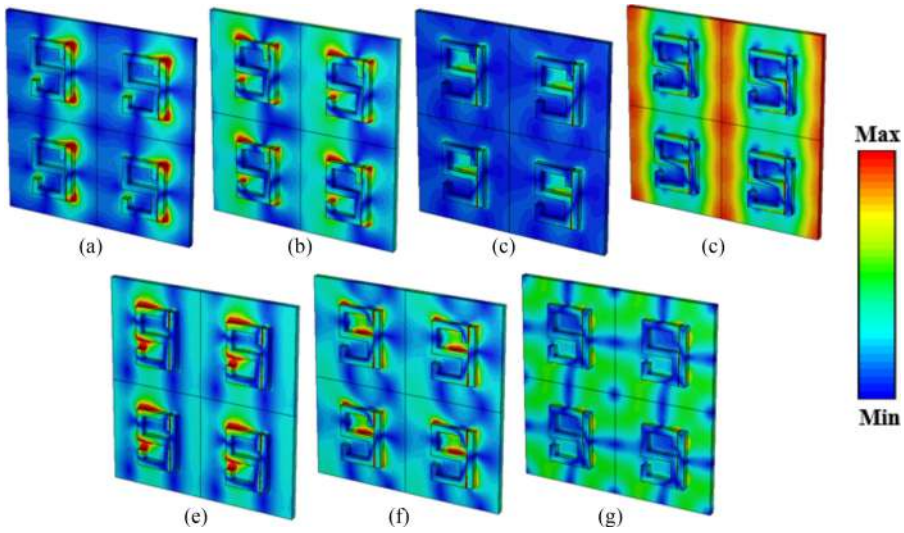

Fig. 7. Electric field distribution patterns of the proposed metasurface at different operating frequencies, namely (a) 2.86 THz, (b) 3.05 THz, (c) 3.33 THz, (d) 3.50 THz, (e) 3.83 THz, (f) 3.88 THz, and (g) 3.90 THz.

appearance of only one PIT peak at nearly 3.59 THz operating frequency, when the metasurface is undergoing the TE-polarized incidence excitation (Fig. 6(d)). But, the use of TM-polarized waves, keeping the other operating conditions fixed, yields three PIT peaks positioned at nearly 3.05 THz, 3.50 THz and 3.88 THz. As such, we observe the rotation of metasurface allows alterations in the magnitude as well as positions of PIT peaks of the resonator structure. The two extreme values of angles, i.e., 0° and 90°, provide the maximum number of transmission peaks corresponding to both the TE- and TM-polarized incidence excitations.

In order to understand the physical behavior of the effect of the observed PIT better, we now look into the electric field distribution patterns corresponding to different transmission dips and peaks in Fig. 2 under the normal incidence of TE-polarized excitation. Within the context, we take into account the frequencies 2.86 THz, 3.05 THz, 3.33 THz, 3.50 THz, 3.83 THz, 3.88 THz, and 3.90 THz; Figs. 7(a)−(g) exhibit the obtained field patterns. Looking at Figs. 7(a), 7(c), 7(e) and 7(g), we notice weak mutual coupling between the rectangular strip and S-shaped resonator – the fact that causes the absence of PIT effect corresponding to the respective operating frequencies. Figs. 7(b), 7(d) and 7(f) exhibit strong coupling between the resonator components, which results in three PIT windows at the respective frequency values.

Fig. 7 shows the 3D plots of the electric fields, wherein the mutual coupling between the rectangular strip and S-shaped resonator can be seen. Within the context, one may be interested in alterations in electric fields at the interfce of the dielectric medium and metasurface, and also, at the top of metasurface. With this viewpoint in mind, we choose some of the cases shown in Fig. 7, namely the frequency values 2.86 THz and 3.05 THz, which correspond to Figs. 7(a) and 7(b), respectively. Using these illustrative values of frequency, Fig. 8 depicts the two-dimensional (2D) electric field patterns at the interface of two mediums (Figs. 8(a) and (b)), and that at the top of metasurface (Figs. 8(c) and (d)). Fig. 8 clearly presents the fields better coupled at the top of metasurface (Figs. 8(c),(d)) than that exist at the interface.

To further explore the phenomenon of PIT in our proposed structure, we also investigate the electric field distributions corresponding to different transmission peaks (centered at the points of the PIT windows) obtained upon rotating the unit cell at an angle of 60° (i.e., $\alpha = 60°$). Also, we consider the case of TE-polarized incidence excitation; Fig. 9 illustrates the obtained results. More explicitly, Figs. 9(a)–(d) show the field patterns corresponding to the PIT peaks positioned at 3.34 THz, 3.88 THz, 4.0 THz and 4.13 THz, respectively. As can be noticed in these figures, the

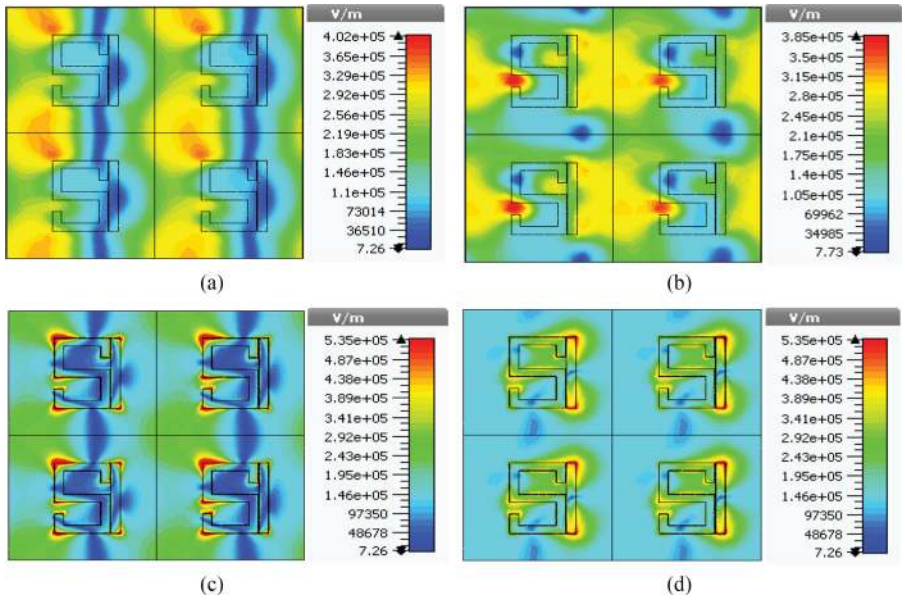

Fig. 8. 2D electric field distributions at the metasurface-dielectric interface corresponding to (a) 2.86 THz, (b) 3.05 THz, and at the top of metasurafce corresponding to (c) 2.86 THz, (d) 3.05 THz. The chosen frequency values are as used in Figs. 7(a) and (b).

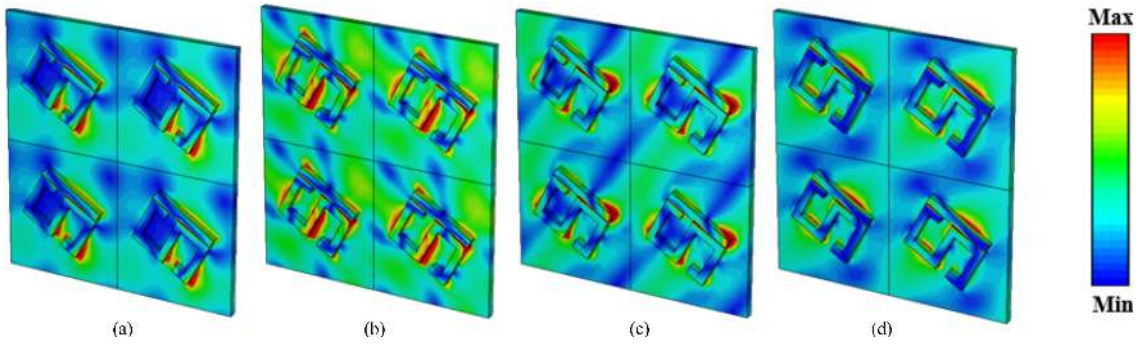

Fig. 9. Electric field distribution patterns of the proposed metasurface under the TE-polarized incidence excitation, and at the operating frequencies (a) 3.34 THz, (b) 3.88 THz, (c) 4.0 THz, and (d) 4.13 THz corresponding to the rotational angle $\alpha = 60°$.

metasurface components (i.e., the S-shaped resonator and rectangular strip) are strongly coupled due to interference. As a result of this mutual coupling, the PIT-like phenomenon is generated at the stated operating frequencies.

Similar to Fig. 8 shown above, we get the illustrative plots corresponding to Fig. 9 as well to observe the electric field patterns at the metasurface-dielectric interface, and also, at the top of metasurface, taking into account the rotational angle $\alpha = 60°$. For this purpose, we take the illustrative frequency values as 3.88 THz and 4.13 THz, that represent the field patterns in Figs. 9(b) and (c), respectively; the corresponding field enhancement profiles at the interface as well as the top of metasurface are shown in Figs. 10(a)−(d). We clearly observe in these figures the mutual coupling of electric fields between the rectangular strip and S-shaped resonator at the top of metasurface; the strength of coupling remains less at the interface.

We now attempt to investigate the effect of the angle of incidence on the transmission spectra, taking into account the situation of both the TE- and TM-polarized incidence excitations. Within the context, Figs. 11 and 12, respectively, illustrate the transmission characteristics corresponding to

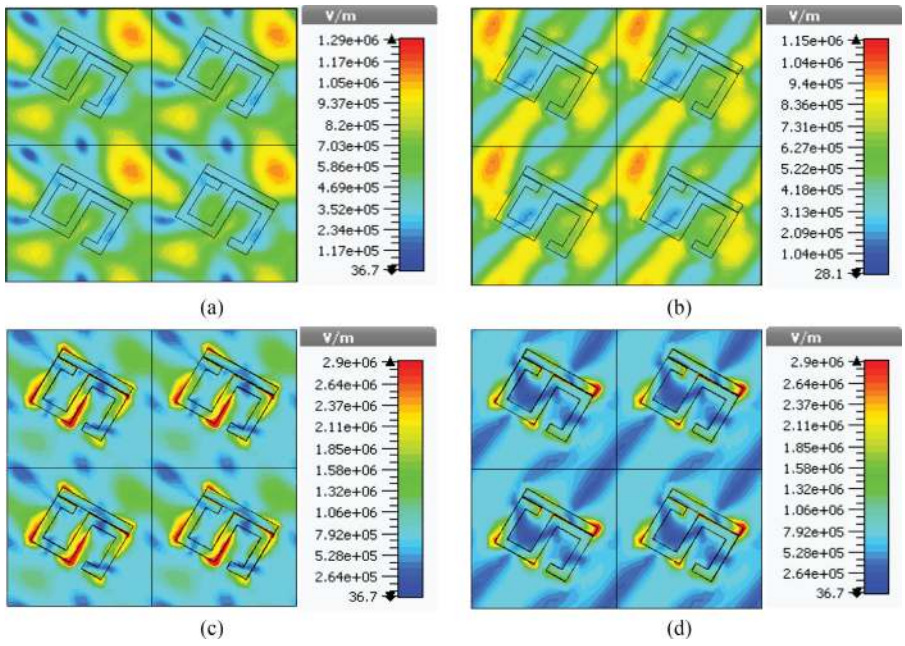

Fig. 10. 2D electric field distributions at the metasurface-dielectric interface corresponding to (a) 3.88 THz, (b) 4.0 THz, and at the top of metasurafce corresponding to (c) 3.88 THz, (d) 4.0 THz. The chosen frequency values are as used in Figs. 9(b) and (c) corresponding to the rotational angle $\alpha = 60°$.

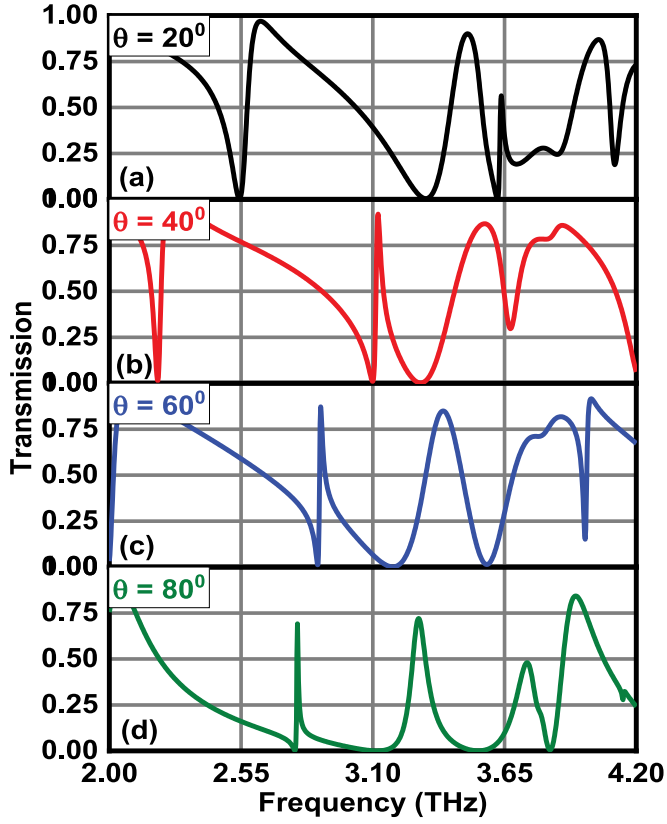

Fig. 11. Transmission spectra under the TE-polarized incidence excitation for angles (a) $\theta = 20°$, (b) $\theta = 40°$, (c) $\theta = 60°$, and (d) $\theta = 80°$.

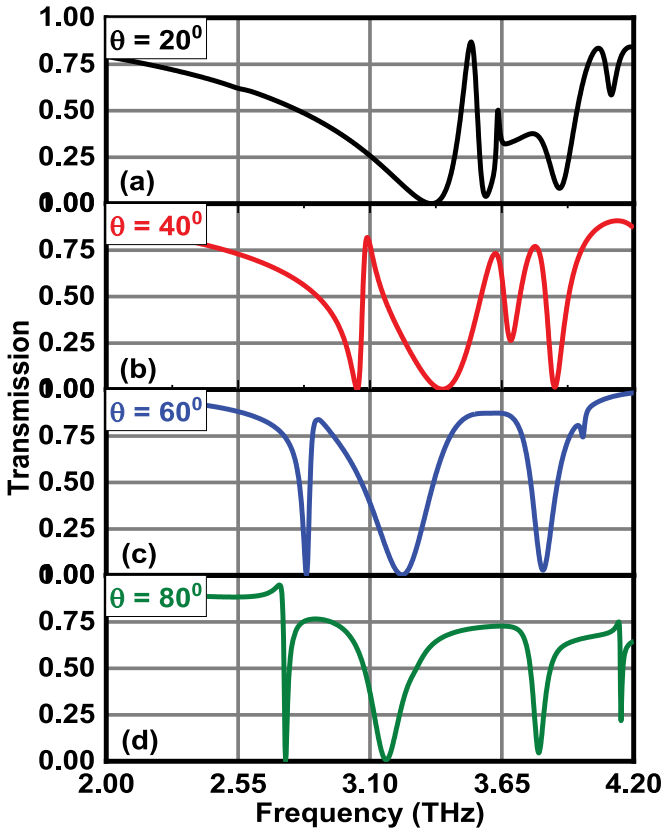

Fig. 12. Transmission spectra under the TM-polarized incidence excitation corresponding to angles (a) $\theta = 20°$, (b) $\theta = 40°$, (c) $\theta = 60°$, and (d) $\theta = 80°$.

the cases of TE- and TM-fields. For this purpose, we use four different values of incidence angles, namely 20°, 40°, 60°, and 80°. We clearly observe the presence of PIT peaks, the features of which essentially depend on the angle of incidence excitation.

In the case of TE-polarized incidence excitation, we observe in Fig. 11(a) that a 20° angle of incidence yields the PIT resonance peaks positioned at the operating frequencies 2.62 THz, 3.49 THz, 3.63 THz, 3.81 THz and 4.04 THz; the PIT peak at 2.62 THz frequency yields the maximum transmission. Upon increasing the angle, red-shifts in the position of transmission peaks happen. For instance, we get the PIT peaks at the frequencies 2.25 THz, 3.12 THz, 3.57 THz, 3.78 THz and 3.89 THz corresponding to 40° angle of incidence (Fig. 11(b)). Looking at the transmission spectra obtained upon a further increase in incidence angle, the red-shift in PIT peaks becomes obvious. In all situations, the magnitude of transmission remains the maximum corresponding to the minimum value of frequency.

It is very important to discuss the quality (Q-) factor associated with the PIT window. The Q-factor is defined as $Q = f_r/FWHM$ with f_r and FWHM being the resonance frequency and full-width half-maximum of the PIT window, respectively. Considering Fig. 11(a), it is determined that the Q-factors corresponding to PIT peaks at 3.5 THz and 3.64 THz are 27 and 485, respectively. Fig. 11(b), that relates to 40° angle of incidence, the Q-factors for PIT peak at 3.13 THz and 3.56 THz are 97 and 17, respectively. The highest value of Q-factor as 557 is attained for the PIT at 2.81 THz, as obtained upon using 80° angle of incidence. It is noteworthy that sharp PIT peak has higher Q-factor, whereas wider PIT peak will have lower value of the same. Higher Q-factor (i.e., sharp peak) in PIT window remains useful for switching and sensing applications.

Fig. 12 depicts the transmission spectra of the proposed metasurface under the TM-polarized incidence excitation, keeping the other geometrical and operational conditions unchanged. We

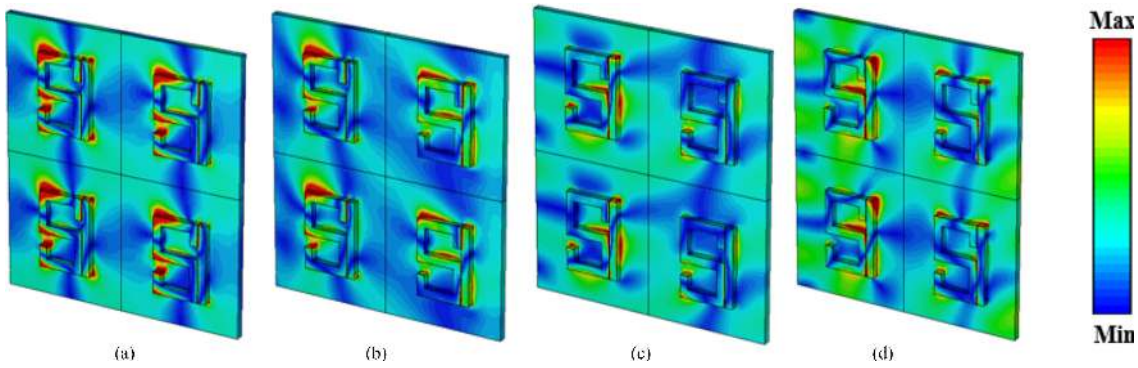

Fig. 13. Electric field distribution patterns of the proposed metasurface under the TE-polarized incidence excitation, and at the operating frequencies (a) 3.12 THz, (b) 3.56 THz, (c) 3.79 THz, and (d) 3.88 THz corresponding to incidence angle $\theta = 40°$.

observe that all the PIT peaks undergo significant amount of red-shifts, as compared to the case of TE-polarized incidence. Further, upon an increase in the angle of incidence, we notice the presence of relatively flat PIT windows in the higher frequency span. The use of 20° angle of incidence yields multiple PIT peaks (Fig. 12(a)) – the feature that becomes more prominent upon increasing the angle to 40°; the situation that gives three PIT peaks positioned at the operating frequency values at nearly 3.08 THz, 3.62 THz and 3.79 THz (Fig. 12(b)). Further increase in incidence angle results in nearly flat band of transmission in the high-frequency regime (Figs. 12(c) and (d)). As such, the more oblique the incidence is, the more will be the chances of attaining flat transmission band by the use of the proposed kind of metasurface. However, this kind of feature was not observed in the case of TE-polarized incidence excitation.

Now, considering the features of *Q*-factor in the case of TM-polarized incidence, we notice that its values are significantly lowered, as compared to what observed before under the TE-field excitation (Fig. 11). For instance, with respect to 40° incidence angle (Fig. 11(b)), we find the values of *Q*-factor as 34, 36 and 35 corresponding to the PIT peaks at 3.089 THz, 3.62 THz and 3.78 THz, respectively. Therefore, it may be inferred that the excitation of TM-mode remains of relatively less importance, as compared to the TE-mode excitation, so far as the applications in the areas of sensing and/or switching are concerned.

To further explore the insignts into the PIT effect, we investigate the electric field profiles of the proposed metasurface under the situation of oblique incidence, as discussed before in Fig. 11(b), which relates to the case of 40° incidence angle. Fig. 13 exhibits the obtained electric field distribution patterns corresponding to the PIT peaks noticed in Fig. 11(b). We find in this figure that the PIT peaks are positioned at the frequencies 3.12 THz, 3.56 THz, 3.79 THz and 3.88 THz; Figs. 13(a)–(d) illustratre the respective electric field distribution patterns. In all these figures, the mutual coupling of electric field with both the resonator components in the unit cell can be easily noticed. However, such a kind of coupling essentially depends upon the horizontal separation *S* (Fig. 1) between the components, which the metasurafce is comprised of. Keeping this in mind, we attempt to evaluate the transmission spectra of the metasurface-based structure under varying values of *S*; Fig. 14 illustrates the obtained results in the case when the TE-polarized waves excite the metasurafce under normal incidence.

As can be seen in Fig. 14, we use five different values of the distance of separation between the S-shaped resonator and rectangular strip in the metasurface; these are as 0.5 μm, 1.0 μm, 1.5 μm, 2.0 μm and 2.5 μm, and the respective transmission characteristics obtained in these situations are depicted in Figs. 14(a)–(e). We observe the existance of three PIT peaks in all the metasurface configurations, and the positions of those remain almost unchanged. However, the values of FWHM of PIT peaks greatly depend on the parameter *S* which, in turn, yields the *Q*-factor. We notice that the first PIT peak is the most prominent one in all the situations, and the corresponding value

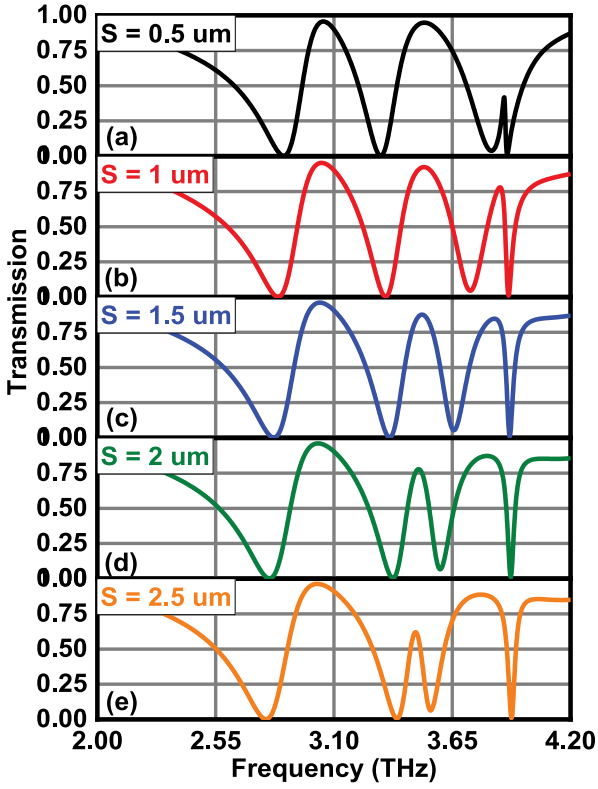

Fig. 14. Transmission spectra obtained under varying distance of separation S, namely (a) 0.5 μm, (b) 1.0 μm, (c) 1.5 μm, (d) 2.0 μm, and (e) 2.5 μm.

of Q-factor reduces with the increase in S. Also, the amplitude of transmission of the second peak reduces, and that of the third peak increases with increasing S. Comparing Figs. 2 and 14, we observe that the former one shows two PIT windows with more than 95% transmission, whereas the later one exhibits such windows with over 97% transmission in certain conditions based of the distance of separation S between the resonator components. The value of Q-factor can be determined accordingly, and therefore, a control over the transmission characteristics can be achieved by suitably adjusting the horizontal distance S between the S-shaped resonator and rectangular strip – a way to tune the PIT window of the proposed metasurface. Therefore, careful adjustment of operating conditions would yield PIT windows on demand.

4. Conclusions

The PIT characteristics of planar metasurafce, comprised of an S-shaped resonator and rectangular strip (both made of silver), is investigated. The excitations of the top metasurface by the TE- and TM-polarized waves are taken into account, and the transmission properties are studied under different operational conditions, viz. the incidence angle, the angle of rotation of metasurface and the separation of metasurface resonator components. It is found that the proposed configuration exhibits three PIT windows under the TE-polarized incidence excitation. This happens owing to the strong mutual coupling of bright-bright modes, generated by the S-shaped resonator and rectangular strip. It is noticed that the angle of incidence and incidence polarization leave profound effect on the Q-factor of the PIT windows. Under the influence of rotational and oblique incidence angles, the metasurface shows multiple PIT windows at different operating frequencies. The obtained transmission spectra reveal red-shift in PIT peaks upon increase in incidence angle in the case of TE-polarized excitation. In the case of TM-polarized waves, the red-shifts in PIT

peaks become more significant, but the PIT windows become flat in the higher frequency regimes – the feature that remains greatly influenced due to the angle of excitation. This characteristic is, however, not obtained in the case of TE-polarized incidence excitation, which makes this case more useful for optical applications. The tuning feature of PIT windows is achieved by varying the horizontal distance between the components of metasurface, which basically determines the coupling of fields among those. It is expected that the proposed PIT-like metasurface configuration can be used in photonic devices, such as buffers, sensors, and memory storage units.

Acknowledgment

The authors are thankful to two anonymous reviewers for constructive criticisms on the manuscript.

References

[1] P. Genevet and F. Capasso, "Holographic optical metasurfaces: A review of current progress," *Repts. Prog. Phys.*, vol. 78, 2015, Art. no. 024401.
[2] S. B. Glybovski, S. A. Tretyakov, P. A. Belov, Y. S. Kivshar, and C. R. Simovski, "Metasurfaces: From microwaves to visible," *Physics Repts.*, vol. 634, pp. 1–72, 2016.
[3] A. M. Shaltout, A. V. Kildishev, and V. M. Shalaev, "Evolution of photonic metasurfaces: From static to dynamic," *J. Opt. Soc. Am. B*, vol. 33, pp. 501–510, 2016.
[4] L. Zhang, S. Mei, K. Huang, and C. W. Qiu, "Advances in full control of electromagnetic waves with metasurfaces," *Adv. Opt. Mat.*, vol. 4, pp. 818–833, 2016.
[5] A. E. Minovich *et al.*, "Functional and nonlinear optical metasurfaces," *Laser & Photon. Rev.*, vol. 9, pp. 195–213, 2015.
[6] N. Yu and F. Capasso, "Flat optics with designer metasurfaces," *Nature Mat.*, vol. 13, pp. 139–150, 2014.
[7] M. R. Tavakol, B. Rahmani, and A. Khavasi, "Terahertz quarter wave-plate metasurface polarizer based on arrays of graphene ribbons," *IEEE Photon. Technol. Lett.*, vol. 31, pp. 931–934, 2019.
[8] D. Wang *et al.*, "Multiband switchable terahertz quarter-wave plates via phase-change metasurfaces," *IEEE Photon. J.*, vol. 8, 2016, Art. no. 5500308.
[9] X. Chen *et al.*, "Longitudinal multifoci metalens for circularly polarized light," *Adv. Opt. Mat.*, vol. 3, pp. 1201–1206, 2015.
[10] M. Khorasaninejad *et al.*, "Polarization-insensitive metalenses at visible wavelengths," *Nano Lett.*, vol. 16, pp. 7229–7234, 2016.
[11] R.-B. Hwang, N.-C. Hsu, and C.-Y. Chin, "A spatial beam splitter consisting of a near-zero refractive index medium," *IEEE Trans. Antennas and Propagat.*, vol. 60, pp. 417–420, 2011.
[12] M. Ghasemi, M. Baqir, and P. K. Choudhury, "On the metasurface-based comb filters," *IEEE Photon. Technol. Lett.*, vol. 28, no. 10, pp. 1100–1103, 2016.
[13] M. Ghasemi and P. K. Choudhury, "Nanostructured concentric gold ring resonator-based metasurface filter device," *Optik*, vol. 127, pp. 9932–9936, 2016.
[14] Z. Li, K. Yao, F. Xia, S. Shen, J. Tian, and Y. Liu, "Graphene plasmonic metasurfaces to steer infrared light," *Sci. Repts.*, vol. 5, 2015, Art. no. 12423.
[15] B. Gerislioglu, A. Ahmadivand, and N. Pala, "Tunable plasmonic toroidal terahertz metamodulator," *Phys. Rev. B*, vol. 97, pp. 161405-1–161405-4, 2018.
[16] A. Ahmadivand, B. Gerislioglu, and Z. Ramezani, "Gated graphene island-enabled tunable charge transfer plasmon terahertz metamodulator," *Nanoscale*, vol. 11, pp. 8091–8095, 2019.
[17] G. Zheng, H. Mühlenbernd, M. Kenney, G. Li, T. Zentgraf, and S. Zhang, "Metasurface holograms reaching 80% efficiency," *Nature Nanotechnol.*, vol. 10, pp. 308–312, 2015.
[18] W. T. Chen *et al.*, "High-efficiency broadband meta-hologram with polarization-controlled dual images," *Nano Lett.*, vol. 14, pp. 225–230, 2014.
[19] Y. -W. Huang *et al.*, "Aluminum plasmonic multicolor meta-hologram," *Nano Lett.*, vol. 15, pp. 3122–3127, 2015.
[20] B. Gholipour, J. Zhang, K. F. MacDonald, D. W. Hewak, and N. I. Zheludev, "An all-optical, non-volatile, bidirectional, phase-change meta-switch," *Adv. Mat.*, vol. 25, pp. 3050–3054, 2013.
[21] H. Ahmed, A. A. Rahim, H. Maab, M. M. Ali, N. Mahmood, and S. Naureen, "Phase engineering with all-dielectric metasurfaces for focused-optical-vortex (FOV) beams with high cross-polarization efficiency," *Opt. Mat. Express*, vol. 10, pp. 434–448, 2020.
[22] H. Liu *et al.*, "Twisted focusing of optical vortices with broadband flat spiral zone plates," *Adv. Opt. Mat.*, vol. 2, pp. 1193–1198, 2014.
[23] B. G. Cai, Y. B. Li, W. X. Jiang, Q. Cheng, and T. J. Cui, "Generation of spatial Bessel beams using holographic metasurface," *Opt. Express*, vol. 23, pp. 7593–7601, 2015.
[24] S. Liu *et al.*, "Anomalous refraction and nondiffractive Bessel-beam generation of terahertz waves through transmission-type coding metasurfaces," *ACS Photon.*, vol. 3, pp. 1968–1977, 2016.
[25] K.-J. Boller, A. Imamoğlu, and S. E. Harris, "Observation of electromagnetically induced transparency," *Phys. Rev. Lett.*, vol. 66, 1991, Art. no. 2593.

[26] S. E. Harris, J. Field, and A. Imamoğlu, "Nonlinear optical processes using electromagnetically induced transparency," *Phys. Rev. Lett.*, vol. 64, 1990, Art. no. 1107.
[27] S. Zhang, D. A. Genov, Y. Wang, M. Liu, and X. Zhang, "Plasmon-induced transparency in metamaterials," *Phys. Rev. Lett.*, vol. 101, 2008, Art. no. 047401.
[28] N. Papasimakis, V. A. Fedotov, N. Zheludev, and S. Prosvirnin, "Metamaterial analog of electromagnetically induced transparency," *Phys. Rev. Lett.*, vol. 101, 2008, Art. no. 253903.
[29] S.-Y. Chiam, R. Singh, C. Rockstuhl, F. Lederer, W. Zhang, and A. A. Bettiol, "Analogue of electromagnetically induced transparency in a terahertz metamaterial," *Phys. Rev. B*, vol. 80, 2009, Art. no. 153103.
[30] D. Phillips, A. Fleischhauer, A. Mair, R. Walsworth, and M. D. Lukin, "Storage of light in atomic vapor," *Phys. Rev. Lett.*, vol. 86, 2001, Art. no. 783.
[31] N. Liu *et al.*, "Planar metamaterial analogue of electromagnetically induced transparency for plasmonic sensing," *Nano Lett.*, vol. 10, pp. 1103–1107, 2010.
[32] D. C. Zografopoulos, M. Swillam, and R. Beccherelli, "Hybrid plasmonic modulators and filters based on electromagnetically induced transparency," *IEEE Photon. Technol. Lett.*, vol. 28, pp. 818−821, 2016.
[33] S. Paul and M. Ray, "Simultaneous switching at multiple wavelengths using plasmon induced transparency and Fano resonance," *IEEE Photon. Technol. Lett.*, vol. 29, pp. 739−742, 2017.
[34] L. Dong, X. Xu, C. Li, Y. Guo, K. Sun, and Y. Ding, "Plasmon-induced transparency in sensing application with semicircle cavity waveguide," *Opt. Commun.*, vol. 410, pp. 751−755, 2018.
[35] A. Alipour, A. Farmani, and A. Mir, "High sensitivity and tunable nanoscale sensor based on plasmon-induced transparency in plasmonic metasurface," *IEEE Sensors J.*, vol. 18, pp. 7047−7054, 2018.
[36] W. Wei, X. Yan, B. Shen, and X. Zhang, "Plasmon-induced transparency in an asymmetric bowtie structure," *Nanoscale Res. Lett.*, vol. 14, 2019, Art. no. 246.
[37] H. Feng *et al.*, "Phase-coupled plasmon-induced transparency in metasurface with periodically arranged bimolecular systems, " *Appl. Surf. Sci.*, vol. 506, 2020, Art. no. 144888.
[38] H.-J. Li, L.-L. Wang, and X. Zhai, "Plasmonically induced absorption and transparency based on MIM waveguides with concentric nanorings," *IEEE Photon. Technol. Lett.*, vol. 28, pp. 1454−1457, 2016.
[39] X. Yan *et al.* "Dynamically controllable plasmon induced transparency based on hybrid metal-graphene metamaterials," *Sci. Repts.*, vol. 7, pp. 1−10, 2017.
[40] D. Shrekenhamer, W. Xu, S. Venkatesh, D. Schurig, S. Sonkusale, and W. J. Padilla, "Experimental realization of a metamaterial detector focal plane array," *Phys. Rev. Lett.*, vol. 109, 2012, Art. no. 177401.
[41] J. D. Baena, S. B. Glybovski, J. P. del Risco, A. P. Slobozhanyuk, and P. A. Belov, "Broadband and thin linear-to-circular polarizers based on self-complementary zigzag metasurfaces," *IEEE Trans. Antennas and Propagat.*, vol. 65, pp. 4124−4133, 2017.
[42] M. Baqir and P. K. Choudhury, "Hyperbolic metamaterial-based UV absorber," *IEEE Photon. Technol. Lett.*, vol. 29, pp. 1548−1551, 2017.
[43] M. Baqir and P. K. Choudhury, "Design of hyperbolic metamaterial-based absorber comprised of ti nanospheres," *IEEE Photon. Technol. Lett.*, vol. 31, pp. 735−738, 2019.
[44] N. A. Olsson, "Lightwave systems with optical amplifiers," *J. Lightwave Technol.*, vol. 7, pp. 1071−1082, 1989.
[45] M. Baqir, A. Farmani, T. Fatima, M. Raza, S. Shaukat, and A. Mir, "Nanoscale, tunable, and highly sensitive biosensor utilizing hyperbolic metamaterials in the near-infrared range," *Appl. Opt.*, vol. 57, pp. 9447−9454, 2018.
[46] A. Ahmadivand, B. Gerislioglu, R. Ahuja, and Y. K. Mishra, "Terahertz plasmonics: The rise of toroidal metadevices towards immunobiosensings," *Mat. Today*, vol. 32, pp. 108−130, 2020.
[47] W. Zhang, Y. Liu, S. Gong, J. Wang, and Y. Jiang, "Wideband RCS reduction of a slot array antenna using phase gradient metasurface," *IEEE Antennas and Wireless Propagat. Lett.*, vol. 17, pp. 2193−2197, 2018.
[48] X. Liu, G. Fu, Y. Wang, P. Pan, and Z. Liu, "Polarization-adjusting ultra-narrow multi-band color filtering by dielectric metamaterials," *IEEE Photon. Technol. Lett.*, vol. 28, pp. 979−982, 2016.
[49] M. A. Baqir *et al.*, "Tunable plasmon induced transparency in graphene and hyperbolic metamaterial-based structure," *IEEE Photon. J.*, vol. 11, 2019, Art. no. 4601510.
[50] Z. Chai, X. Hu, Y. Zhu, F. Zhang, H. Yang, and Q. Gong, "Low-power and ultrafast all-optical tunable plasmon-induced transparency in plasmonic nanostructures," *Appl. Phys. Lett.*, vol. 102, 2013, Art. no. 201119.
[51] S. Zhan, H. Li, Z. He, B. Li, Z. Chen, and H. Xu, "Sensing analysis based on plasmon induced transparency in nanocavity-coupled waveguide," *Opt. Express*, vol. 23, pp. 20313−20320, 2015.
[52] J. Chen, P. Wang, C. Chen, Y. Lu, H. Ming, and Q. Zhan, "Plasmonic EIT-like switching in bright-dark-bright plasmon resonators," *Opt. Express*, vol. 19, pp. 5970−5978, 2011.
[53] Y. Ye, Y. Xie, Y. Liu, S. Wang, J. Zhang, and Y. Liu, "Design of a compact logic device based on plasmon-induced transparency," *IEEE Photon. Technol. Lett.*, vol. 29, pp. 647−650, 2017.
[54] N. Liu, M. Hentschel, T. Weiss, A. P. Alivisatos, and H. Giessen, "Three-dimensional plasmon rulers," *Science*, vol. 332, pp. 1407−1410, 2011.
[55] H. Chen, H. Zhang, M. Liu, Y. Zhao, S. Liu, and Y. Zhang, "Tunable multiple plasmon-induced transparency in three-dimensional Dirac semimetal metamaterials," *Optics Commun.*, vol. 423, pp. 57−62, 2018.
[56] W.-Y. Li, X. Zhai, X.-J. Shang, S.-X. Xia, M. Qin, and L.-L. Wang, "Multi-spectral plasmon induced transparency based on three-dimensional metamaterials," *Optical Mater. Express*, vol. 7, pp. 4269−4276, 2017.
[57] K. Wen *et al.*, "Multiple plasmon-induced transparency responses in a subwavelength inclined ring resonators system," *IEEE Photon. J.*, vol. 7, 2015, Art. no. 4801807.
[58] H.-J. Hagemann, W. Gudat, and C. Kunz, "Optical constants from the far infrared to the x-ray region: Mg, Al, Cu, Ag, Au, Bi, C, and Al_2O_3, " *J. Opt. Soc. Am.*, vol. 65, pp. 742−744, 1975.